

1 **Photochemical grid model implementation and application of VOC, NO_x, and O₃ source apportionment**

2 R. H. F. Kwok¹, K. R. Baker¹, S.L. Napelenok^{1*}, G. S. Tonnesen²

3 1 United States Environmental Protection Agency, 109 T.W. Alexander Drive, Research Triangle Park,
4 NC 27711

5 2 United States Environmental Protection Agency, Region 8, 1595 Wynkoop Street, Denver, CO 80202-
6 1129

7 *Corresponding author. Telephone: 1 (919) 541-1135, Fax: 1 (919) 541-1379, e-mail:

8 Napelenok.Sergey@epa.gov.

9 **Abstract**

10 For the purposes of developing optimal emissions control strategies, efficient approaches are needed to
11 identify the major sources or groups of sources that contribute to elevated ozone (O₃) concentrations.
12 Source-based apportionment techniques implemented in photochemical grid models track sources
13 through the physical and chemical processes important to the formation and transport of air pollutants.
14 Photochemical model source apportionment has been used to track source impacts of specific sources,
15 groups of sources (sectors), sources in specific geographic areas, and stratospheric and lateral boundary
16 inflow on O₃. The implementation and application of a source apportionment technique for O₃ and its
17 precursors, nitrogen oxides (NO_x) and volatile organic compounds (VOC), for the Community Multiscale
18 Air Quality (CMAQ) model are described here. The Integrated Source Apportionment Method (ISAM) O₃
19 approach is a hybrid of source apportionment and source sensitivity in that O₃ production is attributed
20 to precursor sources based on O₃ formation regime (*e.g.*, for a NO_x-sensitive regime, O₃ is apportioned
21 to participating NO_x emissions). This implementation is illustrated by tracking multiple emissions source
22 sectors and lateral boundary inflow. NO_x, VOC, and O₃ attribution to tracked sectors in the application
23 are consistent with spatial and temporal patterns of precursor emissions. The O₃ ISAM implementation
24 is further evaluated through comparisons of apportioned ambient concentrations and deposition

25 amounts with those derived from brute force zero-out scenarios, with correlation coefficients ranging
26 between 0.58 and 0.99 depending on specific combination of target species and tracked precursor
27 emissions. Low correlation coefficients occur for chemical regimes that have strong non-linearity in O₃
28 sensitivity, which demonstrates different functionalities between source apportionment and zero-out
29 approaches. Where appropriate use depends on whether source attribution or source sensitivity is
30 desired.

31 **Key words:** ozone, CMAQ, ISAM, source apportionment, sector contribution, photochemical model,
32 NO_x, VOC, deposition

33

34 **1 INTRODUCTION**

35 Regulatory programs have been in place in the United States for more than 50 years to reduce ambient
36 exposure to ozone (O₃) which has harmful effects on human health and vegetation (Bell et al., 2004; U.S.
37 Environmental Protection Agency (EPA), 2009; National Research Council, 1991). Nevertheless, many
38 areas continue to exceed the national ambient air quality standard (NAAQS) for ozone, and uncertainty
39 remains in both the local and distant sources that contribute to exceedances of the NAAQS. The EPA has
40 set a NAAQS for O₃, where compliance with the NAAQS is determined as the three-year average of the
41 4th highest daily maximum 8-hour average O₃. In areas that violate the NAAQS, the states and tribes
42 must develop plans to attain the NAAQS by reducing emissions of O₃ precursors, including volatile
43 organic compounds (VOC) and nitrogen oxides (NO_x). Additionally, Section 110(a)(2)(D) of the Clean Air
44 Act requires states, in part, to eliminate significant contribution to nonattainment of the NAAQS in other
45 states. To develop effective O₃ attainment plans, it is important to understand the sources of ozone that
46 contribute to violations of the NAAQS. Sources of O₃ can include local sources, long-range transport
47 (Zhang et al. 2008, 2009; Lin et al. 2012), stratospheric intrusion (Langford et al. 2009), and

48 photochemical production of O₃ (PO₃) from a wide variety of biogenic and anthropogenic VOC and NO_x
49 precursors (Haagen-Smit 1954; Lefohn et al 2014). For air quality managers who are tasked with
50 developing the most expeditious and cost effective emissions control strategies, it is useful to have
51 methods to identify the relative importance of sources that contribute to high O₃ concentrations, and to
52 predict how O₃ will respond to reductions in VOC and NO_x precursor emissions. Specifically, it is useful to
53 quantify the relative amount of O₃ originating from specific VOC and NO_x emissions sources (or groups
54 of sources, such as an emissions sector), as well as to distinguish locally produced O₃ from O₃ that is
55 transported from upwind sources. Source sensitivity and apportionment approaches have been used to
56 estimate intercontinental ozone contribution (Anenberg et al., 2010; Sudo and Akimoto, 2007; Zhang et
57 al., 2009), and contribution from specific geographic areas (Tong and Mauzerall, 2008), emissions
58 sectors (Fann et al., 2013; Wang et al., 2009; Ying and Krishnan, 2010), and single sources (Bergin et al.,
59 2008). The Integrated Source Apportionment Method (ISAM) for PM_{2.5} was previously implemented in
60 the Community Multiscale Air Quality (CMAQ) model (Kwok et al., 2013). Here, the ISAM
61 implementation is extended to analysis of O₃ source apportionment. This implementation is compared
62 directly with source sensitivity apportionment approaches to provide confidence in the implementation.

63

64 **2. REVIEW OF OZONE SOURCE APPORTIONMENT METHODS**

65 Various methods have been applied to characterize and quantify the relationship between emission
66 sources and ozone concentrations including statistical methods, model sensitivity simulations, and
67 model source apportionment approaches (Cohan and Napelenok, 2011). Statistical approaches using
68 ambient data trends (Porter et al., 2001) or ambient data paired with emissions source characteristics
69 (Kenski et al., 1995; Scheff and Wadden, 1993) have been used in the past as methods for ozone source
70 attribution. Receptor-based approaches such as the chemical mass balance (CMB) or positive matrix

71 factorization (PMF) receptor models provide information about source attribution to ozone precursors,
72 but not directly to ozone (Buzcu and Fraser, 2006; Chung et al., 1996; Kim et al., 2005; Scheff et al.,
73 1996; Tong et al., 2005). Statistical correlation analyses of the regional ozone pattern and time-lagged
74 correlation analyses have also been used to analyze transport effects (Guinnup and Collom, 1997; Husar
75 and Renard, 1997). These studies concluded that transport of O₃ and precursors could occur over the
76 distance of 300-600 km, but did not clearly differentiate the specific origins of transported ozone or the
77 confounding effects of meteorological factors (Guinnup and Collom, 1997).

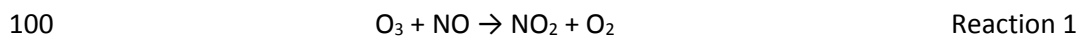
78

79 Air quality model sensitivity simulations have been widely used to predict how O₃ responds to changes in
80 specific sources of emissions of VOC and NO_x (Russell and Dennis, 2000). Source sensitivity approaches
81 include photochemical model “brute force” simulations, in which a single emission source is reduced or
82 removed, and also model extensions that in a single simulation track multiple emissions sensitivities
83 forward (decoupled direct method, DDM) (Dunker et al., 2002) or backward (adjoint) (Mesbah et al.,
84 2012). Model sensitivity approaches have limitations when used for total source culpability, however,
85 because of the nonlinear dependence of O₃ on concentrations of VOC and NO_x. This is especially
86 problematic for evaluating contributions of NO_x because O₃ can have negative sensitivity to NO_x in
87 situations where the ratio of VOC to NO_x is low. Therefore, summing the O₃ change in response to
88 sensitivity simulations for multiple emissions sources can result in difficulty interpreting the cumulative
89 effect of those emissions on O₃.

90 In source apportionment approaches, the objective is to identify the amount of O₃ produced by
91 particular emissions sources rather than determining the sensitivity of O₃ to those sources. This
92 distinction is important in cases where O₃ has a non-linear sensitivity or negative sensitivity to changes
93 in emissions. Source apportionment methods also have the benefit of estimating contributions from

94 many different VOC and NO_x source categories in a single model simulation. To describe the different
95 approaches used in source apportionment methods, it is helpful to review the chemistry of O₃
96 formation. In the troposphere, O₃, nitrogen oxide (NO) and nitrogen dioxide (NO₂) react rapidly in a
97 photo-stationary state (PSS) null cycle, shown in Reactions 1 to 3, which has no net effect on ambient O₃
98 concentrations:

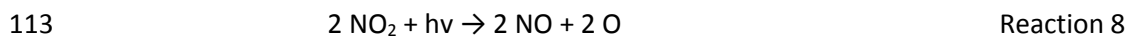
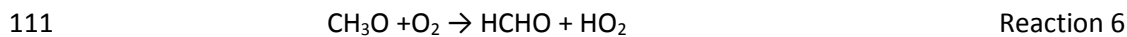
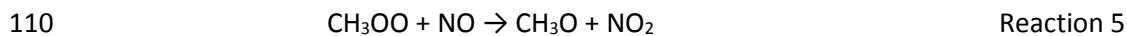
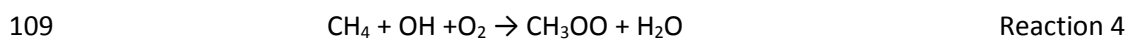
99



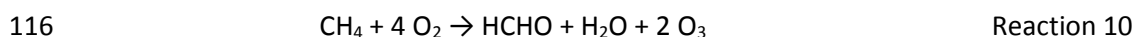
103

104 Photochemical formation of O₃ (PO₃) in the troposphere occurs almost exclusively by the oxidation of
105 VOC (Finlayson-Pitts and Pitts, 1986), as illustrated in Reactions 4 to 7 using methane (CH₄) reactions.
106 While O₃ is not formed directly, Reactions 5 and 7 provide alternate pathways to convert NO to NO₂
107 without the loss of O₃ in Reaction 1, thereby allowing O₃ to accumulate as shown in Reaction 10:

108



115 Net reaction:



117

118 Because multiple families of precursors participate in the photochemical formation of O₃ (PO₃),
119 including NO_x, VOC and free radicals (HO_x=OH+HO₂+RO₂), the developer of a mass apportionment
120 method for sources of PO₃ must determine which precursor is of primary interest for source
121 apportionment. For example, PO₃ can be apportioned only on the basis of the NO_x emissions sources,
122 or VOC emissions sources, or sources of HO_x that contribute to PO₃ in Reactions 4 to 7. Alternatively, a
123 hybrid approach can be used that combines attribution to multiple families of precursors, in which PO₃
124 is attributed to either VOC or NO_x sources depending on whether PO₃ occurs under VOC- or NO_x-
125 sensitive conditions.

126

127 Ozone source apportionment approaches have been implemented in a number of regional air quality
128 models including the Comprehensive Air-quality Model with Extensions (CAMx) (ENVIRON, 2013), the
129 Model for Ozone and Related chemical Tracers (MOZART-4) (Emmons et al., 2012), the Weather
130 Research and Forecasting with Chemistry (WRF-Chem) model (Pfister et al., 2013), and the Community
131 Multiscale Air Quality (CMAQ) model version 4.6 (Arunachalam, 2010; Ying and Krishnan, 2010).

132 Each of the above approaches augments the model by adopting a system of tracer species to track the
133 sources of ozone and its precursor species for selected groupings of emissions categories and
134 geographical regions. It is useful to define the “bulk” concentration as the model simulated
135 concentration of a given species in the unaugmented model, where the bulk concentration should be
136 identical to the sum of the tracers, *e.g.*:

137
$$C_{bulk,O_3}^{i,j,k} = \sum_{n=1}^N C_{O_3n}^{i,j,k} \quad \text{Equation 1}$$

138
$$C_{bulk,VOC}^{i,j,k} = \sum_{n=1}^N C_{VOCn}^{i,j,k} \quad \text{Equation 2}$$

139
140
141
142
143
144
145
146
147
148
149
150
151
152
153
154
155
156
157
158
159
160

$$C_{bulk,NOx}^{i,j,k} = \sum_{n=1}^N C_{NOx_n}^{i,j,k} \quad \text{Equation 3}$$

where N represents the number of tracers needed to represent all sources that contribute to the bulk species concentration, and i,j,k represent cells within the 3-dimensional grid. While each of the models identified above is augmented with a set of tracers, there are significant differences used in source apportionment for these models that are summarized below.

The CAMx Ozone Source Apportionment Technology (OSAT) includes tracers for O_3 and for the families of reactive NO_x and VOC species. The ratio of production of hydrogen peroxide to nitric acid ($PH_2O_2/PHNO_3$) is used to determine if PO_3 occurs in either a NO_x - or VOC-sensitive chemical regime ($PH_2O_2/PHNO_3$ above or below 0.35, respectively; Sillman 1995). If PO_3 occurs in a NO_x -sensitive regime, the NO_x tracers are used to attribute PO_3 proportionally to the emissions sources that contributed to the NO_x concentration. Alternatively, if PO_3 occurs in a VOC-sensitive regime, the VOC tracers are used to attribute PO_3 to the emissions sources that contributed to the VOC concentration. CAMx OSAT does not include tracers for individual VOC species. Instead, to reduce computational cost, the source attribution is based on a VOC family tracer, defined as the reactivity weighted sum of the emissions of individual VOC species for each source category. The VOC tracer decays based on an estimate of its reactivity with OH, and the VOC tracer's contribution to PO_3 is estimated based on its maximum incremental reactivity (MIR) (Carter,1994). The adjustment using MIR also accounts for increased PO_3 from highly reactive VOC, such as aldehydes and aromatics, which can also act as sources of OH radicals (Jeffries and Tonnesen, 1994). O_3 production and destruction reactions operate simultaneously within the chemical mechanism, so the net change in ozone during a chemistry solver time step in the model simulation is the sum of production and loss:

161 $\Delta O_3 = PO_3 + DO_3$ Equation 4

162 where $DO_3 \leq 0$ indicates chemical destruction of O_3 . In CAMx OSAT, PO_3 is estimated as the net change
163 in O_3 during the chemistry time step combined with amount of chemical destruction of O_3 :

164 $PO_3 = \Delta O_3 - DO_3$ Equation 5

165 PO_3 is used to update the O_3 tracers attributed to VOC and NO_x emissions sources, and in a separate
166 step the O_3 tracers are reduced by DO_3 . CAMx OSAT does not consider the reaction of O_3 with NO as
167 chemical destruction, because this reaction occurs as part of the PSS null cycle in Reactions 1 to 3 that
168 neither produces nor destroys O_3 . Finally, it should be noted that CAMx OSAT adopts tracers that are
169 updated at each chemistry time step based on chemical reaction rates, but these tracers are not added
170 to the chemical mechanism and therefore do not increase the computational cost of the numerical
171 chemistry algorithm.

172
173 In contrast to CAMx OSAT, the MOZART and WRF-Chem models both adopt a source apportionment
174 method that augments the chemical mechanism with additional species and duplicative reactions that
175 acts as tracers of emissions sources of NO_x . O_3 tracers are updated based only on their attribution to
176 NO_x . These adaptations are primarily appropriate at the global scale, where PO_3 is primarily NO_x -limited,
177 and tagging NO_x was an appropriate choice for that purpose (Emmons et al., 2012). However, the
178 MOZART and WRF-Chem source apportionment approach treats Reaction 1 as chemical destruction of
179 O_3 , so that when a stratospheric or boundary condition (BC) O_3 molecule reacts with anthropogenic NO
180 molecule via Reaction 1, the O_3 that is subsequently formed in Reactions 2 and 3 is considered
181 anthropogenic. Because the PSS null cycle does not result in any net PO_3 , the approach used in
182 MOZART and WRF-Chem could artificially convert tracers of stratospheric and BC O_3 to anthropogenic O_3
183 and overestimate the contribution of anthropogenic NO_x to O_3 .

184

185 Ying and Krishnan (2010) implemented a source apportionment algorithm in CMAQ that relies on a set
186 of additional species and duplicative reactions that act as tracers of O₃ produced from individual VOC
187 species. In this case, the model developers were primarily concerned with O₃ attribution to
188 anthropogenic and biogenic VOC in the urban ozone non-attainment area, and therefore tracers were
189 only evaluated for VOC species. The algorithm used the NO₂ production rates in Reactions 5 and 7 to
190 represent PO₃, so this method has the benefit of representing total photochemical production of odd
191 oxygen (O_x) which is defined as the sum of O₃, NO₂ and other species that act as a reservoir of atomic
192 oxygen. However, this approach does not consider the effects that highly reactive VOC species have on
193 production of new radical species which also affects the PO₃. Therefore, this approach may
194 underestimate the contribution of high reactivity VOC and overestimate the contribution of low
195 reactivity to PO₃. Additionally, because of the large number of additional tracer species and reactions
196 included in the photochemical mechanism, and the resulting increased computational cost, only one
197 VOC emissions source category could be included in each simulation.

198

199 Ozone source attribution analysis can also be performed using the process analysis and integrated
200 reaction rate outputs in the CMAQ and CAMx models. Each model has the option to store hourly mass
201 throughput for each reaction in the chemical mechanism, and post processing can be performed to
202 attribute ozone to VOC and NO_x precursors when these processes are coupled with tools such as
203 Lagrangian trajectory models to track source specific transport (Henderson et al., 2011). While these
204 approaches are useful for analyzing chemical production terms within selected grid cells, it is
205 computationally challenging to use this approach for source attribution to specific emissions sources
206 across the full model domain.

207

208 Evaluating the accuracy of source apportionment model results is challenging, because source
209 contribution of secondary pollutants cannot be assessed independently based on monitoring data.
210 Previous PM_{2.5} source apportionment implementations have been evaluated by comparing source
211 contributions to changes in PM_{2.5} using brute force source model sensitivity simulations and by
212 evaluating conservation of mass in the source apportionment results (Kwok et al., 2013; Wang et al.,
213 2009). Source apportionment and brute force source sensitivity methods should provide similar results
214 when O₃ has a linear or nearly linear sensitivity to changes in precursors' emissions. Therefore,
215 comparisons to sensitivity simulations can be useful for evaluating source apportionment methods.
216 However, in cases where O₃ has a strong non-linear dependence on precursors, such as the sensitivity to
217 NO_x under radical limited conditions, source apportionment and sensitivity approaches can provide
218 different results. For example, Emmons et al. (2012) found differences of a factor of 2 – 4 when
219 comparing the MOZART O₃ source apportionment method to 20% perturbations in precursor NO_x
220 emissions. Dunker et al. (2002) compared CAMx O₃ source attributions using OSAT and DDM sensitivity
221 simulations and found that the two methods gave similar spatial distributions and that DDM sensitivity
222 simulations explained about 70% of the modelled O₃ concentration. Zhang et al (2005) compared CAMx
223 OSAT, DDM and Process Analysis methods and also found that each method provided generally
224 consistent assessments of source contributions to O₃, with the exception of urban areas in which O₃ had
225 negative sensitivity to NO_x. In each of the studies described above, small emissions reductions or first-
226 order DDM sensitivities do not account for non-linearity in the O₃ response to precursors and may not
227 provide a reliable test for evaluating source apportionment approaches. Tonnesen (1999) found that
228 model sensitivity analyses using small emissions changes did not accurately characterize the effect of
229 uncertainty in model inputs on O₃ attainment strategies and recommended that large emissions changes
230 should be used to assess model sensitivity. Therefore, similar to previous studies, ISAM O₃ contributions

231 are compared here with model sensitivity simulations to determine if ISAM provides generally
232 consistent results. However, instead of using small emissions changes, we use brute force zero-out
233 scenarios of emissions sectors to account more reliably for non-linearity in the O₃ response to changes in
234 precursors. While we expect that there will be some differences in the sensitivity and source
235 apportionment results, especially for strongly non-linear NO_x sensitivity in urban areas, we believe this
236 approach to be useful for evaluating the accuracy of ISAM O₃ source attributions for conditions that do
237 not have strongly non-linear sensitivities.

238

239

240 **3 METHOD**

241 *3.1 Implementation Overview*

242 The ISAM for O₃ has been implemented in the CMAQ version 5.0.2 model, which was developed by the
243 United States Environmental Protection Agency (EPA) and is used by EPA, other regulatory agencies, and
244 academic institutions to characterize local to continental scale ozone formation and transport (Byun and
245 Schere, 2006; Foley et al., 2010). The ISAM O₃ source apportionment implementation is designed to
246 track the contribution from user selected categories of NO_x and VOC emissions to model estimated NO_x,
247 VOC, and ozone concentration and deposition. In addition to precursor emissions, the model tracks O₃,
248 NO_x, and VOC from the lateral boundary conditions, and initial conditions. Precursor emissions tracers
249 can be defined geographically using an additional model input file that assigns the fractional area of
250 each model grid cell to specified sub-regions (typically a State or Province). Precursor emissions tracers
251 can also be defined by source sector (typically, major point sources, mobile sources, biogenic sources,
252 etc.) or for specific point sources with a tag identification environment variable associated with each

253 point source stack on the model ready input file. The user may also combine the emissions source sector
254 and the specific geographic sub-region functionality. This implementation adds to the previous version
255 of PM_{2.5} ISAM code and uses many of the same approaches that were presented in detail by Kwok et al
256 (2013). Only new ozone specific physical and chemical algorithms are described here.

257

258 The ozone source apportionment approach implemented in CMAQ is similar to the approach
259 implemented in CAMx (ENVIRON, 2013), but uses tracers for individual nitrogen and VOC species,
260 whereas CAMx uses two tracers to represent the families of NO_x and VOC. Ozone production is
261 attributed to either VOC or NO_x emissions sources based on the ozone chemical formation regime that is
262 estimated using the PH₂O₂/PHNO₃ indicator ratio, similar to the implementation in CAMx. As described
263 above, the bulk concentration of each VOC and NO_x species is equal to the sum of the tracers used to
264 identify the sources of VOC and NO_x. The bulk O₃ concentration in each model grid cell is equal to the
265 sum of O₃ tracers that were produced in either VOC- or NO_x-sensitive conditions:

266

$$267 \quad O3_{bulk} = \sum_{tag} O3V_{tag} + \sum_{tag} O3N_{tag} \quad \text{Equation 6}$$

268

269 where $O3V_{tag}$ and $O3N_{tag}$ are the VOC-sensitive and NO_x-sensitive O₃ attributed to each tag source,
270 respectively. The implementation described here is for the Carbon Bond 2005 (CB05) photochemical
271 mechanism that uses a reduced set of model VOC species (Yarwood et al, 2005). Tracers are defined for
272 the 14 CB05 VOC species contributing to ozone formation including acetaldehyde (ALD2), higher
273 aldehydes (ALDX), ethene (ETH), ethane (ETHA), ethanol (ETOH), formaldehyde (FORM), internal olefin
274 (IOLE), isoprene (ISOP), methanol (MEOH), olefin (OLE), paraffin (PAR), mono-terpene (TERP), toluene

275 (TOL), and xylene (XYL) (Table 1). The nine nitrogen compounds in CB05 that participate in the O₃
276 formation chemistry include NO, NO₂, nitrogen trioxide (NO₃), dinitrogen pentoxide (N₂O₅), nitrous acid
277 (HONO), peroxyacyl nitrates (PAN), higher peroxyacyl nitrates (PANX), peroxyntic acid (PNA), and
278 organic nitrates (NTR).

279 ISAM apportions CMAQ-calculated wet and dry deposition of O₃, NO_x, and all VOC species into individual
280 sources as done in the previous PM_{2.5} ISAM code. Both of these processes follow simple linear
281 algorithms where the mass removed is a function of existing mass and a removal coefficient and thus
282 did not require additional consideration for the ozone implementation.

283

284 In the CMAQ gas phase chemistry module, nitrogen species are updated by chemical sensitivity
285 approach as in Kwok et al (2013). Likewise, the explicit VOC tracers are entered into the same algorithm
286 in a matrix solution:

$$287 \quad [VOC_{s,tag}^{new}] = (\mathbf{I} - \frac{\Delta t}{2} \mathbf{J})^{-1} (\mathbf{I} + \frac{\Delta t}{2} \mathbf{J}) [VOC_{s,tag}^{old}] \quad \text{Equation 7}$$

288 , where $VOC_{s,tag}^{new/old}$ is the VOC species j for sector tag before (old) or after (new) the Jacobian

289 calculation; \mathbf{I} the identity matrix; \mathbf{J} the Jacobian matrix calculated based on the average of bulk

290 concentrations before and after any gas-phase solver for CB05 model species $\left(\frac{[C_{S,bulk}^{new}] + [C_{S,bulk}^{old}]}{2} \right)$ (e.g.

291 Euler Backward Method, which is used here). This system is solved by decomposing $(\mathbf{I} - \frac{\Delta t}{2} \mathbf{J})^{-1} (\mathbf{I} + \frac{\Delta t}{2} \mathbf{J})$

292 into a product of lower and upper triangular matrices, which is known as LU decomposition. The solution

293 is obtained only once for every model synchronization time step Δt instead of incremental chemical time

294 steps to increase computational efficiency at little expense to accuracy as was previously shown in the

295 original implementation of the CMAQ decoupled direct method (DDM) (Hakami, 2004) .

296

297 *3.2 Ozone Regime Indicators*

298 The ratio of the instantaneous production rates of hydrogen peroxide to nitric acid ($\text{PH}_2\text{O}_2/\text{PHNO}_3$) is
299 used as an indicator to distinguish photochemical regimes, in which PO_3 is primarily sensitive to either
300 VOC or NO_x . Kleinman (1994) evaluated the dependence of H_2O_2 on high and low NO_x photochemical
301 regimes and Sillman (1995) proposed that a ratio of $\text{H}_2\text{O}_2/\text{HNO}_3$ equal to 0.35 should distinguish NO_x -
302 sensitive regimes ($\text{H}_2\text{O}_2/\text{HNO}_3 > 0.35$) versus VOC-sensitive regimes ($\text{H}_2\text{O}_2/\text{HNO}_3 < 0.35$). Sillman (1995)
303 evaluated the modelled daily maximum O_3 sensitivity to VOC and NO_x as a function of the $\text{H}_2\text{O}_2/\text{HNO}_3$
304 ratio and found that transition from VOC-sensitive to NO_x -sensitive regimes occurred at ratios in the
305 range of 0.35 to 0.6, with the higher ratio occurring in aged air masses, in which concentrations of H_2O_2
306 and HNO_3 may have been affected by deposition. Tonnesen and Dennis (2000a,b) evaluated indicators
307 of instantaneous production of O_x (PO_x) and of daily maximum O_3 concentration and found that
308 indicator ratios had mixed performance for daily maximum O_3 concentration because of the effects of
309 background concentrations and deposition. However, Tonnesen and Dennis (2000a) found that
310 $\text{PH}_2\text{O}_2/\text{PHNO}_3$ was an extremely robust indicator for instantaneous PO_x sensitivity. Numerous other
311 studies have evaluated the performance of several different indicator ratios for daily maximum O_3
312 sensitivity to VOC and NO_x (Milford et al., 1994; Lu et al., 1998; Vogel et al., 1999; Sillman et al., 2000;
313 Andreani-Aksoyoglu, 2002; Jimenez and Baldasano, 2004; Liang et al., 2006; Zhang et al., 2009; Peng et
314 al., 2011; Torres-Jordan et al., 2012). While these studies have found variable and sometimes conflicting
315 results for the usefulness of indicator ratios, each evaluated indicators of daily maximum O_3
316 concentration rather than PO_3 . Based on the most commonly used indicator ratio $\text{PH}_2\text{O}_2/\text{PHNO}_3$, ISAM
317 attributes the instantaneous production term PO_3 to either VOC or NO_x tracers.

318

319 Because O₃ production and loss processes occur simultaneously, the total PO₃ and DO₃ terms are
 320 calculated and used to update the O₃ tracers at each time step in the numerical chemistry solver used in
 321 the model, using the same approach as CAMx (ENVIRON, 2013). When PO₃ occurs in any grid cell,
 322 PH₂O₂/PHNO₃ is used to determine if PO₃ is primarily NO_x- or VOC-sensitive (above or below 0.35,
 323 respectively), and the O₃ tracers are updated with the production to intermediate $O3N_{tag}^{middle}$ and
 324 $O3V_{tag}^{middle}$ using:

326 NO_x-sensitive
$$O3N_{tag}^{middle} = O3N_{tag}^{old} + PO3_{bulk} \times \frac{NO_{tag}^{old} + NO2_{tag}^{old}}{\sum_{tag} (NO_{tag}^{old} + NO2_{tag}^{old})}$$
 Equation 8

328 VOC-sensitive
$$O3V_{tag}^{middle} = O3V_{tag}^{old} + PO3_{bulk} \times \frac{\sum_s (VOC_{s,tag}^{old} \times MIR_s)}{\sum_{tag} \sum_s (VOC_{s,tag}^{old} \times MIR_s)}$$
 Equation 9

330 Here, $VOC_{s,tag}^{old}$ is the concentration of VOC species *s* for source sector *tag*. $PO3_{bulk}$ is the production of
 331 ozone in the grid cell. Table 1 lists the maximum incremental reactivity (MIR) for each VOC species *s*,
 332 developed by Carter (1994) and tabulated by ENVIRON (2013), that are used to approximate the relative
 333 ozone forming potential of the VOC species. Carter (1994) also described alternative reactivity methods
 334 such as Maximum Ozone Incremental Reactivity (MOIR), and Equal Benefit Incremental Reactivity (EBIR).
 335 These alternate scales were also evaluated but did not provide significantly different results.

336 Following the ozone production apportionment, subsequent apportionment of ozone destruction
 337 (where DO₃ <= 0) assumes only its depletion in both regimes for each sector:

338
$$O3X_{tag}^{new} = O3X_{tag}^{middle} + DO3_{bulk} \times \frac{O3X_{tag}^{middle}}{\sum_{tag} (O3N_{tag}^{middle} + O3V_{tag}^{middle})}$$
 Equation 10

339 where X is either N or V.

340

341 **4 APPLICATION AND EVALUATION**

342 A model simulation from June 28 to July 5, 2007 for the State of California (CA) using 12 km sized grid
343 cells (79 columns and 106 rows) and 24 vertical layers was used to evaluate the CMAQ ozone ISAM.
344 Anthropogenic emissions inputs were based on the 2008 National Emission Inventory (NEI) version 2
345 (U.S. Environmental Protection Agency, 2013). Year specific emissions were included for electrical
346 generating units. Meteorological inputs were generated using the Weather Research Forecasting (WRF)
347 model (Skamarock et al., 2008). Biogenic VOC and NO_x emissions were estimated with the Biogenic
348 Emissions Inventory System (BEIS) version 3.14 using temperature and solar radiation from the WRF
349 model as inputs to BEIS (Carlton and Baker, 2011). Mexican emissions were projected from a 1999
350 inventory (U.S. Environmental Protection Agency, 2011b). The 12 km model domain was nested in a 36
351 km continental domain, and boundary inflow to the 36 km domain were based on spatially and
352 temporally variant concentration data from a 2007 year-specific annual GEOS-Chem version 8-03-02
353 simulation (Harvard University, 2012).

354 To demonstrate the functionality of ISAM, eight emission sectors were chosen as tracked contributors to
355 ozone formation. The five point source sectors represented electricity generating units (EGU), non-
356 electricity generating units (Non-EGU), wild fires (FIRE), commercial marine (MARINE), and point sources
357 in Mexico (MEX). The three area sources were on-road mobile (ONRD), non-road mobile (NNRD), and
358 biogenic (BIOG). Tracers were also used for O₃, VOC and NO_x from the lateral boundary conditions
359 (BCON) and initial conditions (ICON). Finally, a single additional tracer (OTHR) was used for all remaining
360 emissions categories that were not explicitly tracked. Table 2 displays emission rates of NO_x and
361 aggregated VOC in those sectors. Percentages of the total emissions contributed by each sector are also

362 listed for reference. For the modelled region, the leading NO_x emissions sectors by mass were ONRD
363 (49.1%), NNRD (13.7%) and BIOG (9.1%), though the untracked emissions accounted for 15.8%. VOC
364 emissions were dominated mostly by BIOG (88.9%). ISAM also has the capability to track regional
365 sources with a user-provided map file in IOAPI/netCDF format and specific flagged point sources.
366 Further details of the brute force setup are described in Section 4.2.

367

368 *4.1 Sector contributions*

369 Figure 1 displays spatial plots of individual contributing sectors to ambient O₃ in CA at 16:00 local time
370 on July 5th, 2007. On this day meteorological conditions were generally stagnant, sunny with light
371 northerly to northwesterly winds. The CMAQ model performed well this day with an O₃ bias of 4.7ppb
372 and average error of 9ppb across the domain during daytime hours. Nighttime hours were excluded
373 from ozone analysis, because ISAM was not designed to predict titration events that often occur at night
374 in areas of large NO_x emissions. For this application, the BCON contribution (Figure 1-j) is largest with
375 contribution from 20 to 40 ppb in coastal CA and contributions of 40 to 60 ppb in eastern CA.
376 Contributions from surface emissions sectors including ONRD and NNRD are also notable with
377 contributions to O₃ as much as 64 ppb near urban areas. BIOG emissions were also an important
378 contributor to O₃ with a maximum of 39 ppb in the central valley. The elevated point source emissions
379 sectors of EGU, Non-EGU, MEX, and MARINE contribute relatively less to O₃ at the surface layer. Spatial
380 correspondence is evident among O₃ (Figure 1), NO_x, and VOC concentrations (Supp Figures 1 and 2), as
381 well as NO_x and VOC emissions (Supp Figures 3 and 4) for most sectors suggesting that ISAM is
382 predicting realistic source-signatures. For example, the wild fire in northern CA is reflected in O₃ (Figure
383 1-b), precursor concentrations (Supp Figures 1-b and 2-b) and emissions (Supp Figures 3-b and 4-b). O₃
384 produced from emission in the marine sector is distributed mostly along the coast (Figure 1-h), which is

385 also seen in NO_x and VOC concentrations (Supp Figures 1-h and 2-h). The corresponding marine
386 emission plot tiles (Supp Figures 3-h and 4-h) indicate sources mostly near the San Francisco Bay area
387 and the Port of Los Angeles. BCON contributions are highest at the lateral edges of the domain and in
388 areas of elevated terrain as expected.

389 The ISAM contributions also realistically change in time similar to bulk modelled estimates and ambient
390 measurements. This is demonstrated for two O₃ monitor locations, at Riverside in Figure 2-a and
391 Sacramento in Figure 2-b, where monitor data are displayed with the model simulated ozone and ISAM-
392 attributed data. Each location had data availability at six separate monitoring sites and Figure 2 shows
393 the average measured and modeled quantities. Individual monitor results are shown in Supp Fig 5.
394 Despite clear differences in the ozone formation behaviour at the two locations, including lower O₃
395 concentrations and greater nighttime titration of O₃ by NO_x at the Sacramento monitor, the observed O₃
396 levels at the two sites are reproduced by CMAQ. Results presented in Supplement Fig 5 and Figure 2
397 demonstrate the base model's ability to capture the temporal and regional variability in observed ozone.

398

399 *4.2 ISAM/brute force comparisons*

400 The brute force or zero-out approach was used to provide an estimate of source contribution for
401 comparison with source contribution estimated with the O₃ source apportionment algorithm. The brute
402 force source sensitivity approach determines O₃ response to partial or total removal of an emission
403 sector/region/species of interest, whereas ISAM was used to provide an alternate estimate of source
404 sector/region/species' contribution to O₃. These approaches provide similar results in linear systems
405 and less similar results in more non-linear systems. Therefore, given the nature of these approaches,
406 source estimates will be similar but should never match given the inherent differences in methodology.
407 Throughout this study, three types of brute force emission datasets were constructed for each sector.

408 The first type removes both NO_x and VOC emissions from each tracked source, denoted by “Both-out”.

409 The second one only removes NO_x, denoted “N-out”. The third only removes VOC, denoted by “V-out”.

410 Since the formation regime of boundary inflow O₃ is unknown, the “Both-out” includes zero-out of

411 BCON O₃, NO, NO₂, and the VOCs. The Both-out brute force simulations were used to compare ISAM O₃

412 collectively from both VOC- and NO_x-sensitive regimes. The N-out was used to compare ISAM NO_x-

413 limited O₃ (O3N) as well as ISAM NO_x, while the V-out assessed ISAM VOC-limited O₃ (O3V) as well as

414 ISAM VOC. Bearing in mind that any zero-out run is subtracted from the base case run so that the

415 resulting difference is compared with the corresponding ISAM sector, the remainder of this manuscript

416 will refer to this difference simply as “Both-out”, “N-out” or “V-out”.

417

418 **Ozone**

419 Figure 3 compares ISAM and Both-out results for O₃ from each tracked sector. Data points are daytime-

420 averaged (6 am to 6 pm Pacific Daylight Time) for each grid cell. In general, surface emissions such as

421 BIOG, NNRD and ONRD (Table 2) give rise to higher surface O₃ concentrations attributed to these

422 sectors. Negative O₃ brute force response in Non-EGU, ONRD, and MEX (Figures 3-c, e, and f) implies a

423 disbenefit (i.e., O₃ increase) from removing both NO_x and VOC emissions from these sectors. This is

424 consistent with previous model sensitivity studies which show disbenefits for NO_x emissions reductions,

425 especially in urban areas that have typically low VOC/NO_x ratios (Jimenez and Baldasano 2004; Zhang et

426 al 2009). ISAM is designed to track sources that contribute to O₃ production, and Figure 3-e shows that

427 even in cases where O₃ has a negative sensitivity to changes in ONRD emissions in certain grid cells,

428 those emissions in an unperturbed environment contribute to O₃ production.

429

430 The high BCON O₃ attribution by ISAM and Both-out shows notable inflow of O₃ from the boundaries as
431 shown more clearly in the stacked bar charts in Figure 4. The global scale GEOS-Chem model is used to
432 provide the O₃ BC, and therefore, source attribution of O₃ would also have to be used in GEOS-Chem to
433 identify the sources that contribute to O₃ inflow at the boundary. However, ISAM predicts systematically
434 more BCON O₃ than the Both-out case. By comparing domain-averaged daily total O₃ of all sectors
435 (including unspecified emissions OTHR) among ISAM, Both-out and CMAQ bulk concentrations (Figure
436 4), it is evident that the sum of ISAM contributions closely matches the bulk O₃, but the sum of zero-out
437 contributions is significantly lower than the bulk ozone concentration (15% lower on average). While
438 ISAM appears to conserve bulk mass as designed, the zero-out case shifts the chemical system into
439 another part of the non-linear, often negative, O₃ response to source change. Similar qualitative
440 features are also exhibited in total O₃ deposition (Supp Figures 6 and 7).

441 Perhaps one of the most substantial ISAM/Both-out comparison contrasts lies in the BIOG sector, in
442 which ISAM sometimes attributes approximately half as much O₃ as Both-out. Previous studies have also
443 found strong nonlinearity in the model response to biogenic emissions (Chameides et al., 1988).
444 Biogenic VOC emissions are generally large in rural areas with low NO_x emissions where O₃ is less
445 sensitive to changes in VOC emissions in these areas. Yet the dominance of biogenic VOC alone cannot
446 adequately explain the ISAM/Both-out discrepancy.

447 Another CMAQ diagnostic tool called decoupled direct method in three dimensions with high order
448 terms (HDDM-3D)(Napelenok et al 2008) was also used to calculate the biogenic O₃ contribution. The
449 output of CMAQ-HDDM provides both first and second order O₃ sensitivity to a perturbation in the
450 biogenic sector, which is then scaled to 100% emissions rates. With all-hour samples averaged, Figure 5
451 shows that the first order DDM approximation explains only 67% of the brute force response, while the
452 second order DDM approximation explains 88% of the zero-out response. This results suggests a highly

453 nonlinear system in which a zero-out difference is the least likely to compare well with the source
454 apportionment results.

455

456 **NO_x**

457 In addition to estimating O₃ contribution from precursors, ISAM also allows for tracking precursor NO_x to
458 model estimated nitrogen containing species concentration and deposition. Figure 6 shows ISAM/N-out
459 NO_x scatter plots for individual sectors. For the modelled region, the most dominant sector is ONRD,
460 followed by NNRD and MARINE, as shown more clearly in stacked bar plots in Figure 7. Expectedly, the
461 order in maximum NO_x concentrations in those sectors is similar to that in the domain-total NO_x
462 emissions (Table 2), in which ONRD and NNRD NO_x emissions dominate. It is interesting to note that the
463 high NO_x concentrations in ONRD, NNRD and MARINE sectors are where VOC/NO_x emissions ratios are
464 low. Conversely, the low NO_x concentration in BIOG sector is where a very large VOC/NO_x emissions
465 ratio occurs.

466 All sectors have correlation coefficients of above 0.90 for the NO_x comparison (Figure 6). Qualitative
467 features in total NO_x deposition (Supp Figures 8 and 9) are also similar to those of the corresponding
468 ambient concentrations (Figures 6 and 7).

469

470 **VOC**

471 Figure 8 shows ISAM/V-out scatter plots of carbon-weighted VOC for individual sectors, which is
472 calculated from ISAM-output VOC species:

473

474

$$V_{tag} = \sum_s VOC_{s,tag} \times NCARB_s \quad \text{Equation 11}$$

475

, where V_{tag} is the aggregated VOC for each tag; $VOC_{s,tag}$ ISAM-output CB05 species s for each tag;

476

and $NCARB_s$ the number of carbon atoms in species s (See Table 1 for the complete list).

477

Correlations are high in most sectors except for EGU and MARINE (Figure 8-g and 8-h), but magnitudes

478

are also small for these two sectors. While BIOG is the most dominant VOC sector, the high maximum

479

VOC concentrations from FIRE do not necessarily lead to a bigger share in the domain-averaged VOC

480

concentration (Figure 9). In fact, domain-wide major VOC sectors are BIOG, BCON and ONRD (Figure 9).

481

Similar features are evident in the total VOC deposition (Supplement Figures 10 and 11).

482

To more closely examine the evolution of individual VOC species in BIOG, BCON and ONRD sectors,

483

daytime domain-averaged ambient concentrations and daily total deposition of individual VOC species

484

are displayed (Supplement Figures 12-a, 12-c, 13-a, 13-c, 14-a and 14-c). Further, we explore the

485

influence of gas-phase degradation of those VOCs by calculating ISAM and V-out contributions from the

486

three sectors while turning off the gas and aerosol chemistry. The corresponding VOC breakdowns were

487

also displayed in Supplement Figures 12-b, 12-d, 13-b, 13-d, 14-b and 14-d. Prior to gas-phase chemistry,

488

VOC portions are very similar between ISAM and V-out in all the three sectors. Although evolution

489

characteristics of the VOC species with photochemistry are different across these sectors, secondary

490

formation of acetaldehyde ALD2, high aldehydes ALDX, and formaldehydes FORM is evident in BIOG and

491

ONRD emissions sectors where primary emissions of the aldehydes are low. These results are consistent

492

with the modelled VOCs' degeneration into formaldehyde (or higher aldehydes) as illustrated in

493

Reactions 4 through 6. On the other hand, the evolution of BCON's aldehydes is more complicated, since

494

both imported and secondarily formed aldehydes can be equally important, none of which were

495

explicitly distinguished by ISAM.

496

497 **5 SUMMARY & DISCUSSION**

498 General similarities between ISAM and zero-out cases establish credibility of the ISAM results, while
499 specific differences, whether in magnitude or in relative portions, demonstrate different functionalities
500 of the two approaches. The choice of appropriate methodology depends on whether source
501 sector/region attribution or sensitivity is of interest Implementation of O₃ tracking capability in CMAQ-
502 ISAM for the CB05 gas-phase chemical mechanism adopts the two-regime approach, with nitrogen and
503 VOC species explicitly tracked through all chemical transport model science processes to facilitate
504 analysis of their chemical and physical transformations. Brute force zero-out CMAQ model simulations
505 serve as a reference to compare the ISAM results applied for a California application in the summer of
506 2007. In general, correlations between ISAM/zero-out estimates are high for both ambient
507 concentration and deposition of O₃ for the major emissions sectors. ISAM estimates of NO_x are higher
508 than nitrogen-out in most sectors except boundary condition. And ISAM VOC estimates are similar when
509 compared to VOC-out in most sectors except EGU and MARINE. Differences between ISAM and zero-out
510 were found in the tracking of O₃ from biogenic emissions, where the model sometimes predicts half of
511 the contribution indicated by zero-out. In the condition of extremely low NO emissions in this sector,
512 high nonlinearity in the gas phase chemistry, supported by the pronounced difference between DDM-
513 based apportionment using 1st order sensitivity coefficients and using 1st and 2nd order coefficients, was
514 found to be responsible for this discrepancy.

515

516 Explicit VOC tracking, available in ISAM, also provides new opportunities to analyze species-specific
517 ozone formation mechanisms (see Supp Figs). This approach not only complements results derived from
518 receptor-based models such as CMB and PMF, but also offers a diagnostic tool to track the chemical
519 evolution of the VOC species that cannot be otherwise adequately explained by receptor-based models

520 alone. In addition to providing VOC contribution information similar to a receptor based source
521 apportionment model, this source-based approach also estimates contribution for nitrogen species, O₃,
522 and deposition of each.

523 The source apportionment technique is recommended when an assessment of contributing sources is
524 desired for model predicted species. Where the change in air quality resulting from perturbing
525 contributing sources is desired then a source sensitivity approach such as brute-force or DDM may be
526 more appropriate. Further, source apportionment should generally be applied for sources or source
527 groups that are well characterized since limitations in the emissions inventory will manifest in
528 photochemical model and source contribution estimates.

529 **5 CODE AVAILABILITY**

530 The implementation of the ISAM source apportionment technique for O₃ and its precursors in the CMAQ
531 photochemical grid model presented here is freely available online at <https://www.cmascenter.org>. This
532 includes code, documentation, and a small test case for benchmarking and illustrating ISAM setup and
533 capability.

534

535 **Disclaimer**

536 Although this work was reviewed by EPA and approved for publication, it may not necessarily reflect
537 official Agency policy.

538 **Acknowledgements**

539 The authors would like to recognize the contribution of David Wong, Lara Reynolds, Allan Beidler, James
540 Beidler, Chris Allen, and Heather Simon.

541 **References**

- 542 Andreani-Aksoyoglu, S., Keller, J., Prevot, Andre, 2002. Applicability of Indicator-Based Approach to
543 Assess Ozone Sensitivities: A Model Study in Switzerland. *Air Pollution Modelling and Simulation*, 21-29.
- 544 Anenberg, S.C., Horowitz, L.W., Tong, D.Q., West, J.J., 2010. An Estimate of the Global Burden of
545 Anthropogenic Ozone and Fine Particulate Matter on Premature Human Mortality Using Atmospheric
546 Modeling. *Environmental Health Perspectives* 118, 1189-1195.
- 547 Arunachalam, S., 2010. Peer Review of Source Apportionment Tools in CAMx and CMAQ. UNC-Chapel
548 Hill, Contract no. EP-D-07-102, Assignment no. 2-06, Version 2.
- 549 Bell, M.L., McDermott, A., Zeger, S.L., Samet, J.M., Dominici, F., 2004. Ozone and short-term mortality in
550 95 US urban communities, 1987-2000. *Journal of the American Medical Association* 292, 2372-2378.
- 551 Bergin, M.S., Russell, A.G., Odman, M.T., Cohan, D.S., Chameides, W.L., 2008. Single-Source Impact
552 Analysis Using Three-Dimensional Air Quality Models. *Journal of the Air & Waste Management*
553 *Association* 58, 1351-1359.
- 554 Buzcu, B., Fraser, M.P., 2006. Source identification and apportionment of volatile organic compounds in
555 Houston, TX. *Atmospheric Environment* 40, 2385-2400.
- 556 Byun, D., Schere, K.L., 2006. Review of the governing equations, computational algorithms, and other
557 components of the models-3 Community Multiscale Air Quality (CMAQ) modeling system. *Applied*
558 *Mechanics Reviews* 59, 51-77.
- 559 Carlton, A.G., Baker, K.R., 2011. Photochemical modeling of the Ozark isoprene volcano: MEGAN, BEIS,
560 and their impacts on air quality predictions. *Environmental Science & Technology*, 45, 4438-4445.
- 561 Carter, W.P.L., 1994. Development of ozone reactivity scales for volatile organic compounds. *Journal of*
562 *the Air and Waste Management Association* 44, 881-899.
- 563 Chameides, W. L., Lindsay, R. W., Richardson, J., Kiang, C. S. 1988. "The role of biogenic hydrocarbons in
564 urban photochemical smog - Atlanta as a case-study." *Science* 241(4872): 1473-1475.
- 565 Chung, J., Wadden, R.A., Scheff, P.A., 1996. Development of ozone-precursor relationships using VOC
566 receptor modeling. *Atmospheric Environment* 30, 3167-3179.
- 567 Cohan, D.S., Hakami, A., Hu, Y., Russell, A.G. (2005). Nonlinear response of ozone to emissions: Source
568 apportionment and sensitivity analysis. *Environmental Science & Technology*, 39: 6739-6748
- 569 Cohan, D.S., Napelenok, S.L., 2011. Air Quality Response Modeling for Decision Support. *Atmosphere* 2,
570 407-425.
- 571 Dunker, A.M., Yarwood, G., Ortmann, J.P., Wilson, G.M., 2002. Comparison of source apportionment
572 and source sensitivity of ozone in a three-dimensional air quality model. *Environmental Science &*
573 *Technology* 36, 2953-2964.

574 Emmons, L.K., Hess, P.G., Lamarque, J.F., Pfister, G.G., 2012. Tagged ozone mechanism for MOZART-4,
575 CAM-chem and other chemical transport models. *Geoscientific Model Development* 5, 1531-1542.

576 ENVIRON, 2013. User's Guide Comprehensive Air Quality Model with Extensions. ENVIRON International
577 Corporation, Novato, California, www.camx.com.

578 Fann, N., Fulcher, C.M., Baker, K.R., 2013. The recent and future health burden of air pollution
579 apportioned across 23 US sectors. *Environmental Science & Technology*.

580 Foley, K. M., Roselle, S. J., Appel, K. W., Bhave, P. V., Pleim, J. E., Otte, T. L., Mathur, R., Sarwar, G.,
581 Young, J. O., Gilliam, R. C., Nolte, C. G., Kelly, J. T., Gilliland, A. B., Bash, J. O. 2010. "Incremental testing
582 of the Community Multiscale Air Quality (CMAQ) modeling system version 4.7." *Geosci. Model Dev.* 3(1):
583 205-226.

584 Finlayson-Pitts, B.J. and J.N. Pitts, Jr. 1986. *Atmospheric Chemistry: Fundamentals and Experimental*
585 *Techniques*. New York: Wiley-Interscience Publication. 1098pp.

586 Guinnup, D. and Collom, B., 1997. Final Report, Vol. I: Executive Summary, OTAG Air Quality Analysis
587 Workgroup. (http://capita.wustl.edu/otag/reports/aqafinvol_1/animations/v1_exsumanimb.html)

588 Husar, R and Renard, W, 1997. Ozone as a function of local wind direction and wind speed: Evidence of
589 local and regional transport. (<http://capita.wustl.edu/otag/Reports/OTAGWIND/OTAGWIND.html>)

590 Jeffries, H.E., Tonnesen, S., 1994. A comparison of two photochemical reaction mechanisms using a
591 mass balance and process analysis. *Atmospheric Environment* 28, 2991-3003.

592 Mathur, R., Sarwar, G., Young, J.O., Gilliam, R.C., Nolte, C.G., Kelly, J.T., Gilliland, A.B., Bash, J.O., 2010.
593 Incremental testing of the Community Multiscale Air Quality (CMAQ) modeling system version 4.7.
594 *Geoscientific Model Development* 3, 205-226.

595 Haagen-Smit, A.J, Fox, M.M., 1954. Photochemical Ozone Formation with Hydrocarbons and Automobile
596 Exhaust. *Air Repair*, 4:3, 105-136, DOI: 10.1080/00966665.1954.10467649.

597 Hakami, A., Odman, M.T., Russell, A.G., 2004. Nonlinearity of the tropospheric ozone production.
598 *Journal of Geophysical Research*, 109, D15303, doi:10.10292003JD004502.

599 Harvard University, 2012. GEOS-Chem Overview.
600 http://acmg.seas.harvard.edu/geos/geos_overview.html.

601 Henderson, B. H., Kimura, Y., McDonald-Buller, E., Allen, D. T., Vizuete, W., 2011. Comparison of
602 Lagrangian Process Analysis tools for Eulerian air quality models. *Atmos. Environ.* 45(29): 5200-5211.

603 Jimenez, P., Baldasano, J.M., 2004. Ozone response to precursor controls in very complex terrains: Use
604 of photochemical indicators to assess O₃-NO_x-VOC sensitivity in the northeastern Iberian Peninsula.
605 *Journal of Geophysical Research*, 109, D20309, doi: 10.1029/2004JD004985.

606 Kenski, D.M., Wadden, R.A., Scheff, P.A., Lonneman, W.A., 1995. Receptor Modeling Approach to VOC
607 Emission Inventory Validation. *Journal of Environmental Engineering-Asce* 121, 483-491.

608 Kim, E., Brown, S.G., Hafner, H.R., Hopke, P.K., 2005. Characterization of non-methane volatile organic
609 compounds sources in Houston during 2001 using positive matrix factorization. *Atmospheric*
610 *Environment* 39, 5934-5946.

611 Kleinman, L., Lee, Y-N., Springston, S.R., Nunnermacker, L., Zhou, X., Brown, R., Hallock, K., Klotz, P.,
612 Leahy, D., Lee, J.H., Newman, L., 1994. Ozone formation at a rural site in the southeastern United States.
613 *Journal of Geophysical Research*, 99, D2, 3469-3482.

614 Kwok, R.H.F., Napelenok, S.L., Baker, K.R., 2013. Implementation and evaluation of PM2.5 source
615 contribution analysis in a photochemical model. *Atmospheric Environment* 80, 398-407.

616 Langford, A. O., Aikin, K. C., Eubank, C. S., Williams E. J., 2009, Stratospheric contribution to high surface
617 ozone in Colorado during springtime, *Geophysical Research Letter*, 36, L12801,
618 doi:10.1029/2009GL038367.

619 Lefohn, A. S. , Emery, C., Shadwick, D., Wernli, H., Jung, J., Oltmans, S. J., 2014. Estimates of background
620 surface ozone concentrations in the United States based on model-derived source apportionment,
621 *Atmospheric Environment*, Volume 84, 275-288, <http://dx.doi.org/10.1016/j.atmosenv.2013.11.033>.

622 Liang, J., Jackson, B., Kaduwela, A., 2006. Evaluation of the ability of indicator species ratios to
623 determine the sensitivity of ozone to reductions in emissions of volatile organic compounds and oxides
624 of nitrogen in northern California. *Atmospheric Environment* 40, 5156-5166.

625 Lin, M., Fiore, A.M., Horowitz, L.W., Cooper, O.R., Naik, V., Holloway, J., Johnson, B.J., Middlebrook,
626 A.M., Oltmans, S.J., Pollack, I.B., Ryerson, T.B., Warner, J.X., Wiedinmyer, C., Wilson, J., Wyman, B.,
627 2012, Transport of Asian ozone pollution into surface air over the western United States in spring,
628 *Journal of Geophysical Research*, 117, D00V07, doi:10.1029/2011JD016961.

629 Lu, C.-H., and J. Chang, 1998, On the indicator-based approach to assess ozone sensitivities and emission
630 features, *J. Geophys. Res.*, 103, 3453–3462.

631 Mesbah, S.M., Hakami, A., Schott, S., 2012. Improving NOx Cap-and-Trade System with Adjoint-Based
632 Emission Exchange Rates. *Environmental Science & Technology* 46, 11905-11912.

633 Milford, J. B., Gao, D. F., Zafirakou, A., Pierce, T. E., 1994. Ozone precursor levels and responses to
634 emissions reductions - analysis of regional oxidant model results. *Atmos. Environ.* 28(12): 2093-2104.

635 Napelenok, S.L., Cohan, D.S., Odman, M.T., Tonse, S., 2008. Extension and evaluation of sensitivity
636 analysis capabilities in a photochemical model. *Environmental Modelling Software*, 23(8): 994-999.

637 National Research Council 1991. Rethinking the ozone problem in urban and regional air pollution.
638 National Academy Press, Washington D.C.

639 Peng, Y-P, Chen, K-S, Wang, H-K, Lai, C-H, Lin, M-H, Lee, C-H., 2011. Applying model simulation and
640 photochemical indicators to evaluate ozone sensitivity in southern Taiwan. *Journal of Environmental*
641 *Sciences*, 23(5), 790-797.

642 Pfister, G., S. Walters, L. Emmons, D.P. Edwards, and J. Aise, 2013: Quantifying the contribution of
643 inflow on surface ozone over California during summer 2008. *Journal of Geophysical Research-*
644 *Atmospheres*, 118, 12282-12299, DOI: 10.1002/2013JD020336

645 Porter, P.S., Rao, S.T., Zurbenko, I.G., Dunker, A.M., Wolff, G.T., 2001. Ozone air quality over North
646 America: Part II - An analysis of trend detection and attribution techniques. *Journal of the Air & Waste*
647 *Management Association* 51, 283-306.

648 Russell, A., Dennis, R. 2000. NARSTO critical review of photochemical models and modeling.
649 *Atmospheric Environment* 34, 2283-2324.

650 Scheff, P.A., Wadden, R.A., 1993. Receptor Modeling of Volatile Organic-Compounds. 1. Emission
651 Inventory and Validation. *Environmental Science & Technology* 27, 617-625.

652 Scheff, P.A., Wadden, R.A., Kenski, D.M., Chung, J., Wolff, G., 1996. Receptor model evaluation of the
653 southeast Michigan ozone study ambient NMOC measurements. *Journal of the Air & Waste*
654 *Management Association* 46, 1048-1057.

655 Sillman, S., 1995. The user of NO_y, H₂O₂, and HNO₃ as indicators for ozone-NO_x-hydrocarbon sensitivity in
656 urban locations. *Journal of Geophysical Research*, Vol 100, No. D7, pp 14175-14188.

657 Skamarock, W. C., Klemp, J. B., Dudhia, J., Gill, D. O., Barker, D. M., Duda, M. G., Huang, X. Y., Wang, W.,
658 Powers, J. G. (2008). A description of the advanced research WRF version 3. National Center for
659 Atmospheric Research, Boulder, Colorado. **NCAR/TN-475**.

660 Sudo, K., Akimoto, H., 2007. Global source attribution of tropospheric ozone: Long-range transport from
661 various source regions. *Journal of Geophysical Research-Atmospheres* 112.

662 G.S. Tonnesen, 1999. Effects of uncertainty in the reaction of the hydroxyl radical with nitrogen dioxide
663 on model-simulated ozone control strategies, *Atmospheric Environment*, 33(10): 1587–1598.

664 Tonnesen, G. S., Dennis, R. L., 2000. Analysis of radical propagation efficiency to assess ozone sensitivity
665 to hydrocarbons and NO_x 1. Local indicators of instantaneous odd oxygen production sensitivity. *J.*
666 *Geophys. Res.-Atmos.* 105(D7): 9213-9225.

667 Tonnesen, G. S., Dennis, R. L., 2000. Analysis of radical propagation efficiency to assess ozone sensitivity
668 to hydrocarbons and NO_x 2. Long-lived species as indicators of ozone concentration sensitivity. *J.*
669 *Geophys. Res.-Atmos.* 105(D7): 9227-9241.

670 Tong, D.Q., Kang, D.W., Aneja, V.P., Ray, J.D., 2005. Reactive nitrogen oxides in the southeast United
671 States national parks: source identification, origin, and process budget. *Atmospheric Environment* 39,
672 315-327.

673 Tong, D.Q., Mauzerall, D.L., 2008. Summertime State-Level Source-Receptor Relationships between
674 Nitrogen Oxides Emissions and Surface Ozone Concentrations over the Continental United States.
675 *Environmental Science & Technology* 42, 7976-7984.

676 Torres-Jardon, R., Garcia-Reynoso, J.A., Jazcilevich, A., Ruiz-Suarez, L.G., Keener, T.C., 2012. Assessment
677 of the Ozone-Nitrogen Oxide-Volatile Organic Compound Sensitivity of Mexico City through an Indicator-

678 Based Approach: Measurements and Numerical Simulations Comparison. Journal of Air & Waste
679 Management Association, 59, 1155-1172.

680 U.S. Environmental Protection Agency, 2009. Integrated Review Plan for the Ozone National Ambient Air
681 Quality Standards Review, EPA-452/D-09-001.

682 chaU.S. Environmental Protection Agency, 2011b. North American Emissions Inventories - Mexico.
683 <http://www.epa.gov/ttnchie1/net/mexico.html>.

684 U.S. Environmental Protection Agency, 2013. The National Emissions Inventory: 2008 National Emissions
685 Inventory Data, <http://www.epa.gov/ttnchie1/net/2008inventory.html>.

686 Vogel, B., Riemer, N., Vogel, H., Fiedler, F., 1999. Findings on NO_y as an indicator for ozone sensitivity
687 based on different numerical simulations. Journal of Geophysical Research, 104, D3, 3605-3620.

688 Wang, X., Li, J., Zhang, Y., Xie, S., Tang, X., 2009. Ozone source attribution during a severe photochemical
689 smog episode in Beijing, China. Science in China Series B-Chemistry 52, 1270-1280.

690 Wang, Z. S., Chien C.-J., and Tonnesen, G.S., 2009. Development of a tagged species source
691 apportionment algorithm to characterize three-dimensional transport and transformation of precursors
692 and secondary pollutants, J. Geophys. Res., 114, D21206, doi:10.1029/2008JD010846.

693 Yarwood, G., Rao, S., Yocke, M., Whitten, G.Z., 2005. Updates to the carbon bond chemical mechanism:
694 CB05. Final Report to U.S.EPA, RT-04-00675.

695 Ying, Q., Krishnan, A., 2010. Source contributions of volatile organic compounds to ozone formation in
696 southeast Texas. Journal of Geophysical Research-Atmospheres 115.

697 Zhang, L., Jacob, D.J., Boersma, K.F., Jaffe, D.A., Olson, J.R., Bowman, K.W., Worden, J.R., Thompson,
698 A.M., Avery, M.A., Cohen, R.C., Dibb, J.E., Flock, F.M., Fuelberg, H.E., Huey, L.G., McMillan, W.W., Singh,
699 H.B., Weinheimer, A.J., 2008. Transpacific transport of ozone pollution and the effect of recent Asian
700 emission increases on air quality in North America: An integrated analysis using satellite, aircraft,
701 ozonesonde, and surface observations, Atmospheric Chemistry and Physics, 8, 6117–6136,
702 doi:10.5194/acp-8-6117-2008.

703 Zhang, L., Jacob, D.J., Kopacz, M., Henze, D.K., Singh, K., Jaffe, D.A., 2009. Intercontinental source
704 attribution of ozone pollution at western US sites using an adjoint method. Geophysical Research Letters
705 36.

706 Zhang, Y., Vijayaraghavan, K., Seigneur, C., 2005. Evaluation of three probing techniques in a three-
707 dimensional air quality model. Journal of Geophysical Research-Atmospheres 110.

708 Zhang, Y., Wen, X-Y, Wang, K., Vijayaraghavan, K., Jacobson, M.Z., 2009. Probing into regional O₃ and
709 particulate matter in the United States: 2. An examination of formation mechanisms through a process
710 analysis technique and sensitivity study. Journal of Geophysical Research 114. D22305,
711 doi:10.1029/2009JD011900.

712

713

714

715

716

717

Table 1. Maximum Incremental Reactivity in CB05 VOC species on ozone production.

| CB05 VOC name | CMAQ acronym | Number of carbon atoms | MIR |
|------------------|--------------|------------------------|-------|
| Acetaldehyde | ALD2 | 2 | 4.45 |
| Higher aldehydes | ALDX | 2 | 6.81 |
| Ethene | ETH | 2 | 4.37 |
| Ethane | ETHA | 2 | 0.11 |
| Ethanol | ETOH | 2 | 1.04 |
| Formaldehyde | FORM | 1 | 4.50 |
| Internal olefin | IOLE | 4 | 13.11 |
| Isoprene | ISOP | 5 | 11.56 |
| Methanol | MEOH | 1 | 0.36 |
| Olefin | OLE | 2 | 8.24 |
| Paraffin | PAR | 1 | 0.32 |
| Monoterpenes | TERP | 10 | 8.82 |
| Toluene | TOL | 7 | 2.94 |
| Xylene | XYL | 8 | 14.79 |

Table 2. All-hour domain averaged NOx and VOC emissions rates for Californian 12-km domain during Jun 28-Jul 5, 2007.

| Emissions Sectors | NOx emis mole/s | % of total NOx emis | VOC emis moleC/s | % of total VOC emis | VOC/NOx moleC/mole |
|---|--------------------|------------------------|---------------------|------------------------|-----------------------|
| BEIS (<i>BIOG</i>) | 76.3 | 9.1 | 20939.2 | 88.9 | 274.4 |
| Marine (<i>MARINE</i>) | 28.7 | 3.4 | 7.5 | 0.0 | 0.3 |
| Fire (<i>FIRE</i>) | 10.7 | 1.3 | 312.7 | 1.3 | 29.2 |
| Nonroad (<i>NNRD</i>) | 115.4 | 13.7 | 469.7 | 2.0 | 4.1 |
| Onroad (<i>ONRD</i>) | 413.7 | 49.1 | 535.7 | 2.3 | 1.3 |
| Mexican point sources (<i>MEX</i>) | 6.6 | 0.8 | 6.6 | 0.0 | 1.0 |
| Elec. Gen. Units (<i>EGU</i>) | 21 | 2.5 | 2.1 | 0.0 | 0.1 |
| Non Elec. Gen. Units (<i>Non-EGU</i>) | 36.9 | 4.4 | 25.5 | 0.1 | 0.7 |
| Untraced emissions (<i>OTHR</i>) | 133.1 | 15.8 | 1264.9 | 5.4 | 9.5 |
| Emissions Totals | 842.4 | | 23563.9 | | 28.0 |

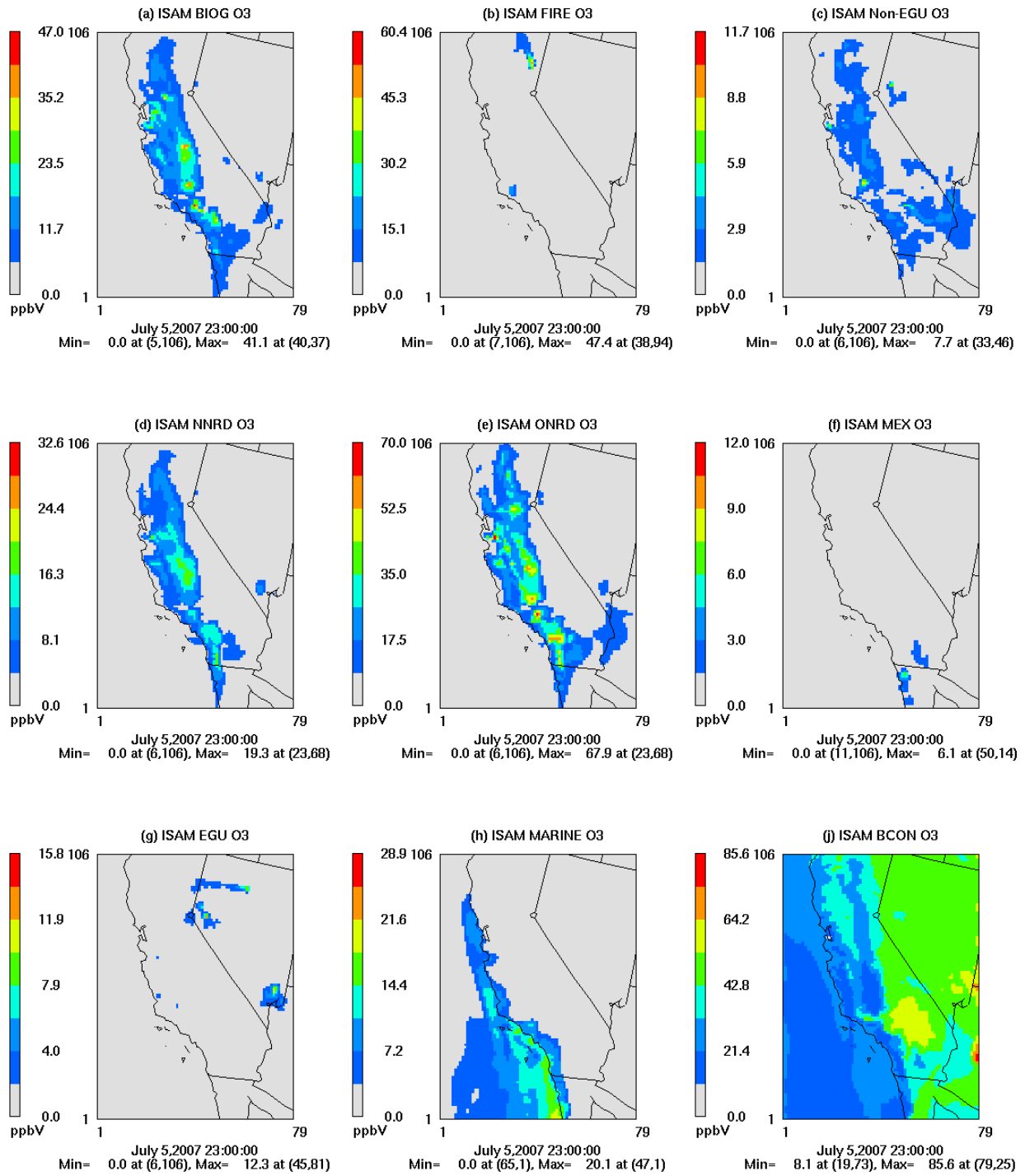


Figure 1. Spatial tiles of 9 source sectors contributing to ambient O₃, at 23UTC (16 PDT) July 5, 2007. (a) biogenic BIOG, (b) wild fires FIRE, (c) non-electricity generation units Non-EGU, (d) non-road mobile NNRD, (e) on-road mobile ONRD, (f) Mexican point sources MEX, (g) electricity generation units EGU, (h) marine MARINE, and (j) boundary conditions BCON. Note different scales across the tiles.

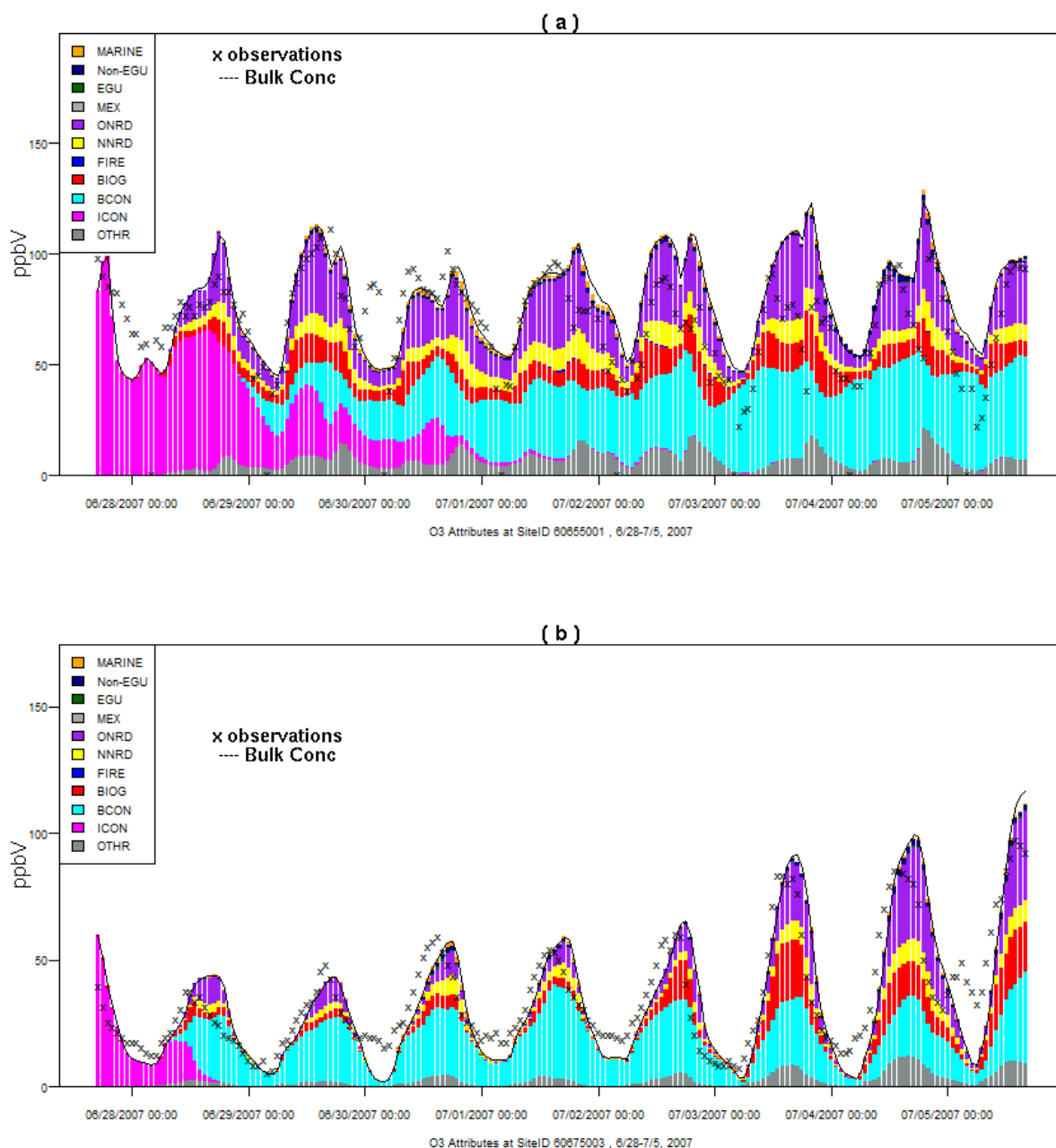


Figure 2. Hourly time series of O₃ observations (crosses) at sites of California Air Resources Board monitoring network; and the corresponding CMAQ-ISAM sector breakdowns (stacking colored bars). Locations are (a) Riverside and (b) Sacramento. The colors represent sector sources: marine (MARINE orange), non-electricity generation units (Non-EGU deep blue), electricity generation units (EGU green), other point sources (MEX light grey), on-road mobile (ONRD purple), non-road mobile (NNRD yellow), wild fires (FIRE blue), biogenic (BIOG red), boundary conditions (BCON cyan), initial conditions (ICON magenta), and remaining unspecified emissions (OTHR grey). The solid black trace on top of the bars denotes the modeled bulk O₃ concentration.

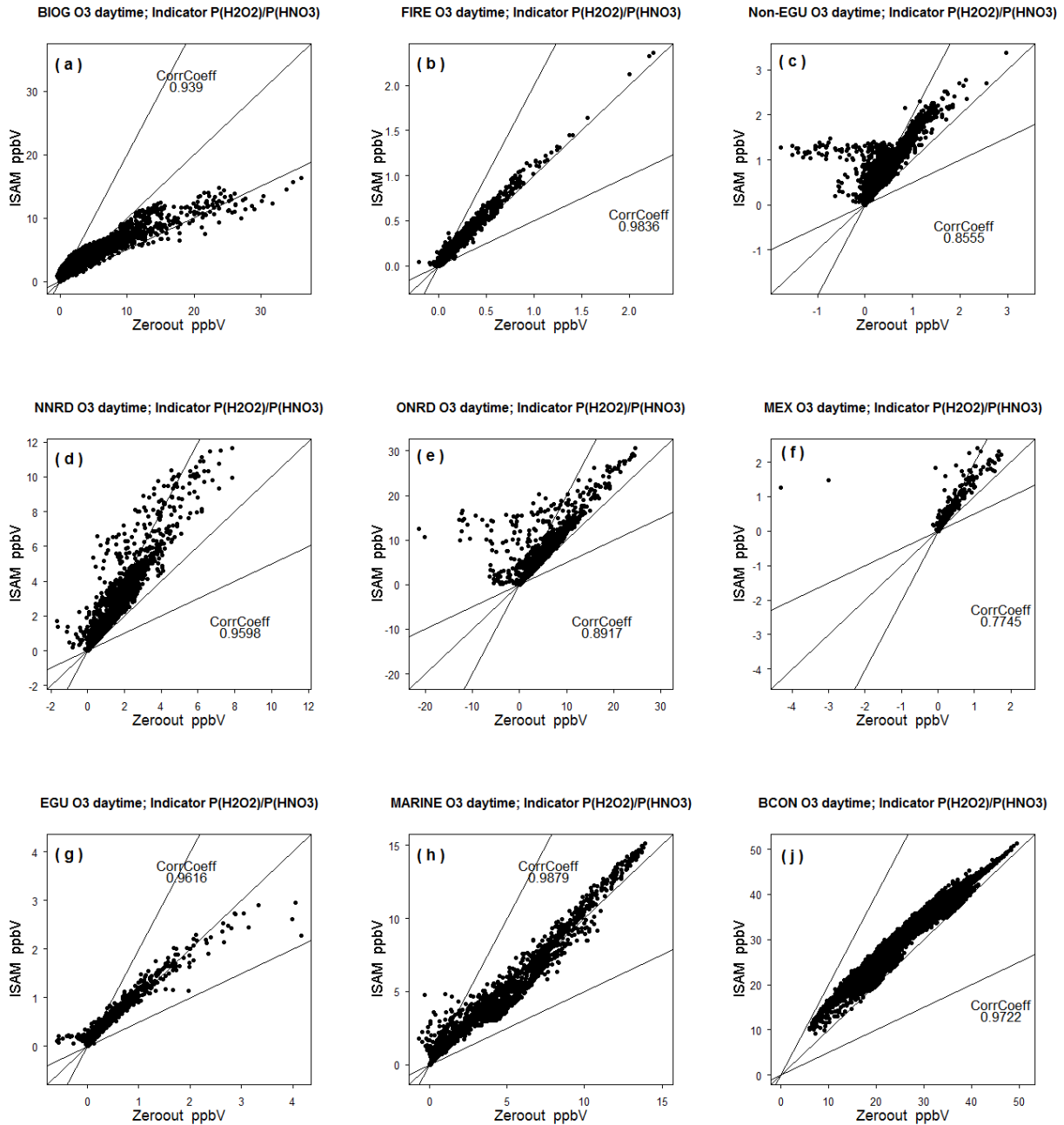


Figure 3. ISAM/both-out O₃ comparison for each sector during daytime hours. The sectors are: (a) biogenic BIOG, (b) wild fires FIRE, (c) non-electricity generation units Non-EGU, (d) non-road mobile NNRD, (e) on-road mobile ONRD, (f) other point sources MEX, (g) electricity generation units EGU, (h) marine MARINE, and (j) boundary conditions BCON. Note different scales across the panels.

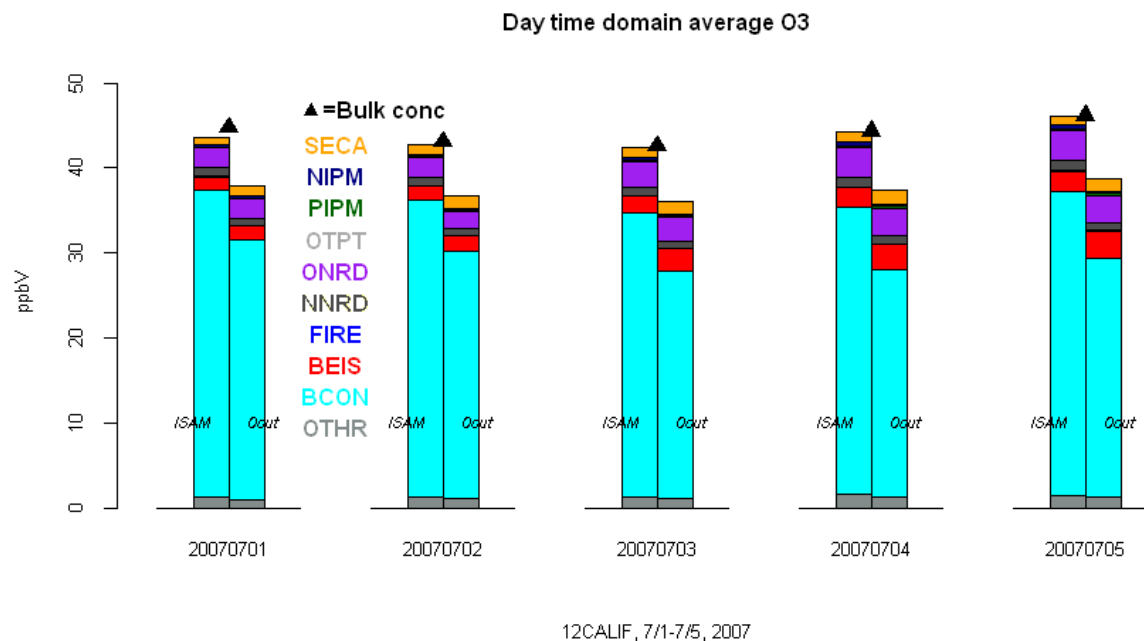
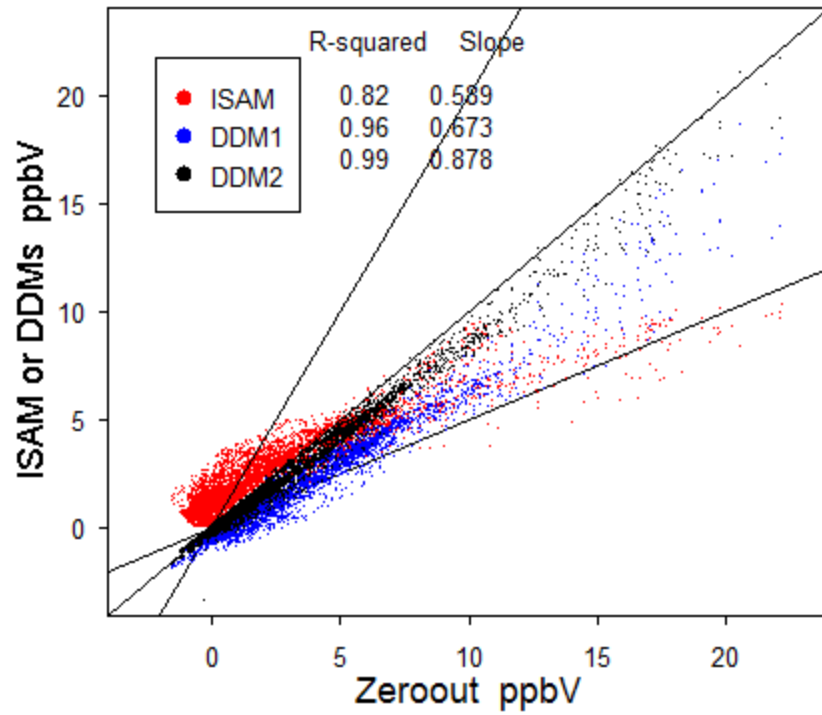


Figure 4. Daytime domain-averaged ambient O₃, July 1-5, 2007 (June 28-30 excluded due to large initial conditions influence). In the bar plot, each day consists of two stacked columns (ISAM on the left; Both-out total on the right) and above them a black triangle designating bulk ambient concentration calculated from regular CMAQ. The colors represent sector sources: marine (MARINE orange), non-electricity generation units (Non-EGU deep blue), electricity generation units (EGU green), other point sources (MEX light grey), on-road mobile (ONRD purple), non-road mobile (NNRD yellow), wild fires (FIRE blue), biogenic (BIOG red), boundary conditions (BCON cyan), and remaining unspecified emissions (OTHR grey).

BIOG O3



Averaged 6/28 - 7/5 2007

Figure 5. Scatter plots of biogenic O₃ with respect to the zero-out brute force, sampled on all-hour-averaged data. Red: ISAM, blue: first order decoupled direct method (DDM1), black: second order decoupled direct method (DDM2). The corresponding R-squared values and regression slopes are also displayed.

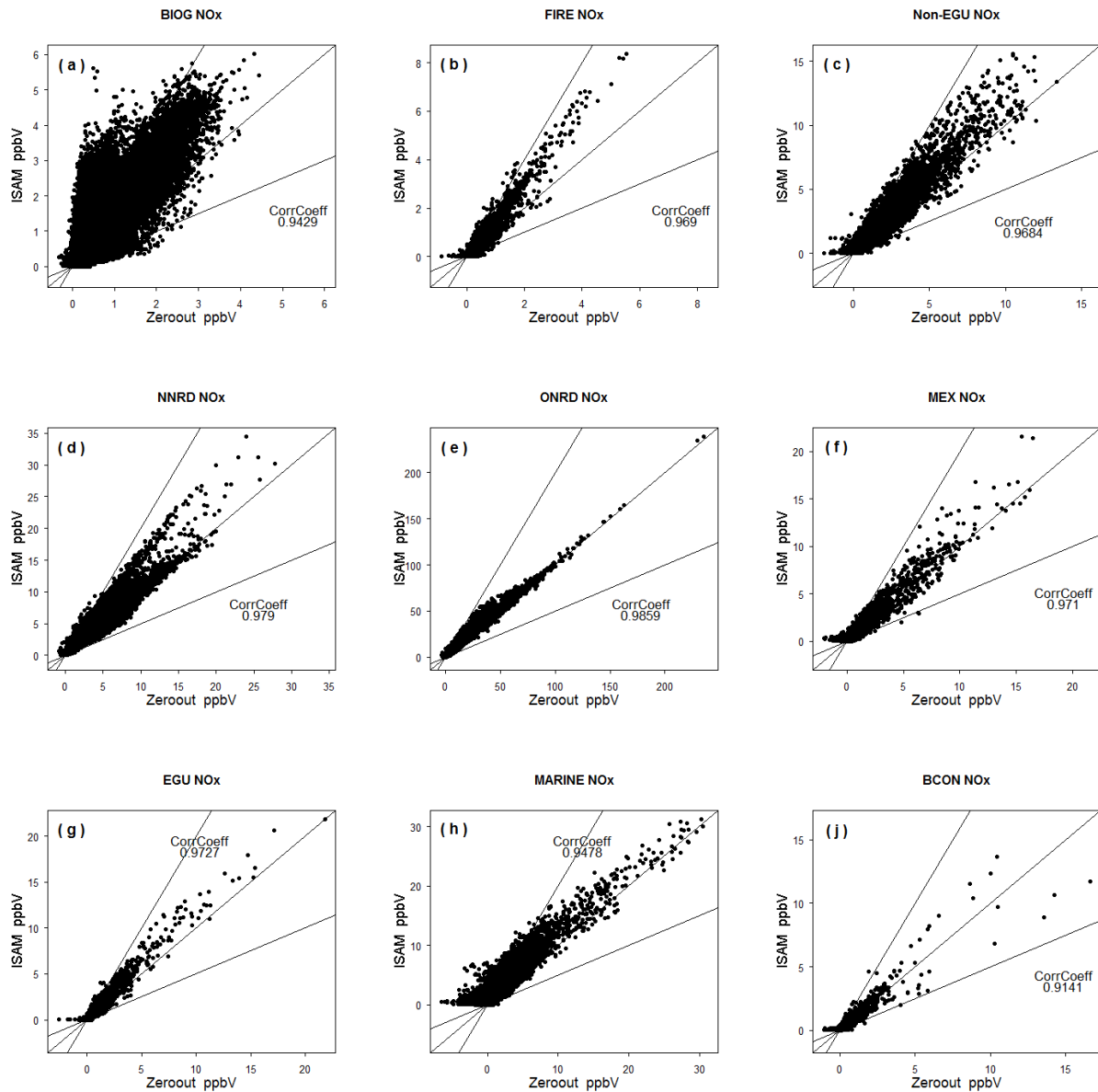


Figure 6. ISAM/N-out NO_x (NO+NO₂) comparison for each sector and all simulated hours. The sectors are: (a) biogenic BIOG, (b) wild fires FIRE, (c) non-electricity generation units Non-EGU, (d) non-road mobile NNRD, (e) on-road mobile ONRD, (f) other point sources MEX, (g) electricity generation units EGU, (h) marine MARINE, and (j) boundary conditions BCON. Note different scales across the panels.

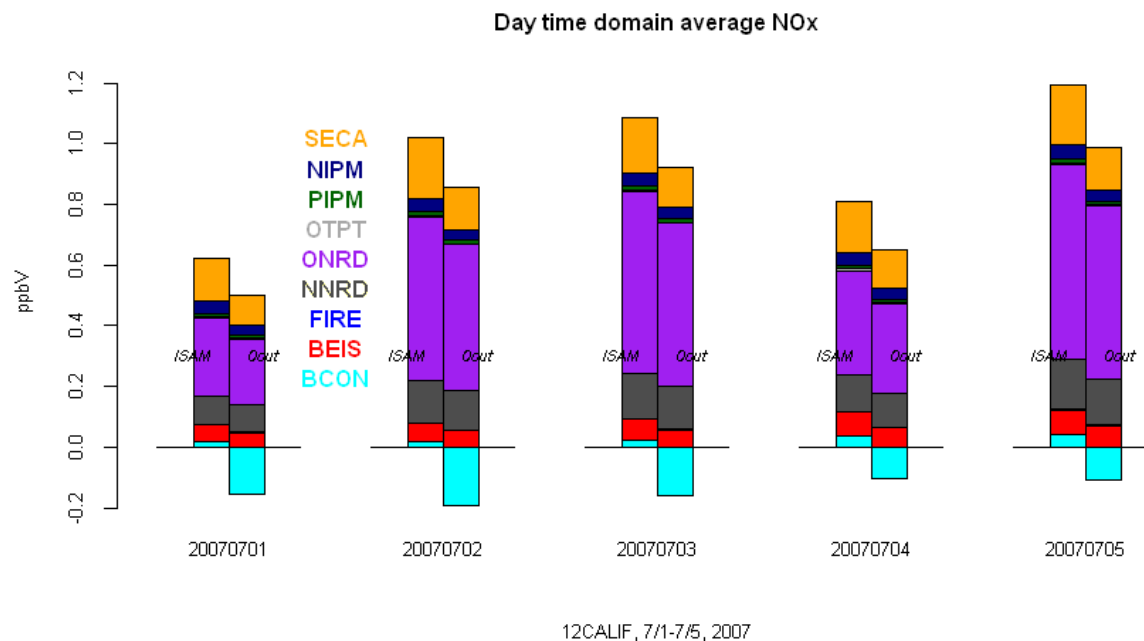


Figure 7. Daytime domain-averaged ambient NOx (NO+NO₂), July 1-5, 2007 (June 28-30 excluded due to large initial conditions influence). As in Fig. 4, for each day left column designates ISAM total, and right one the zero-out. . The colors represent sector sources: marine (MARINE orange), non-electricity generation units (Non-EGU deep blue), electricity generation units (EGU green), other point sources (MEX light grey), on-road mobile (ONRD purple), non-road mobile (NNRD yellow), wild fires (FIRE blue), biogenic (BIOG red), and boundary conditions (BCON cyan).

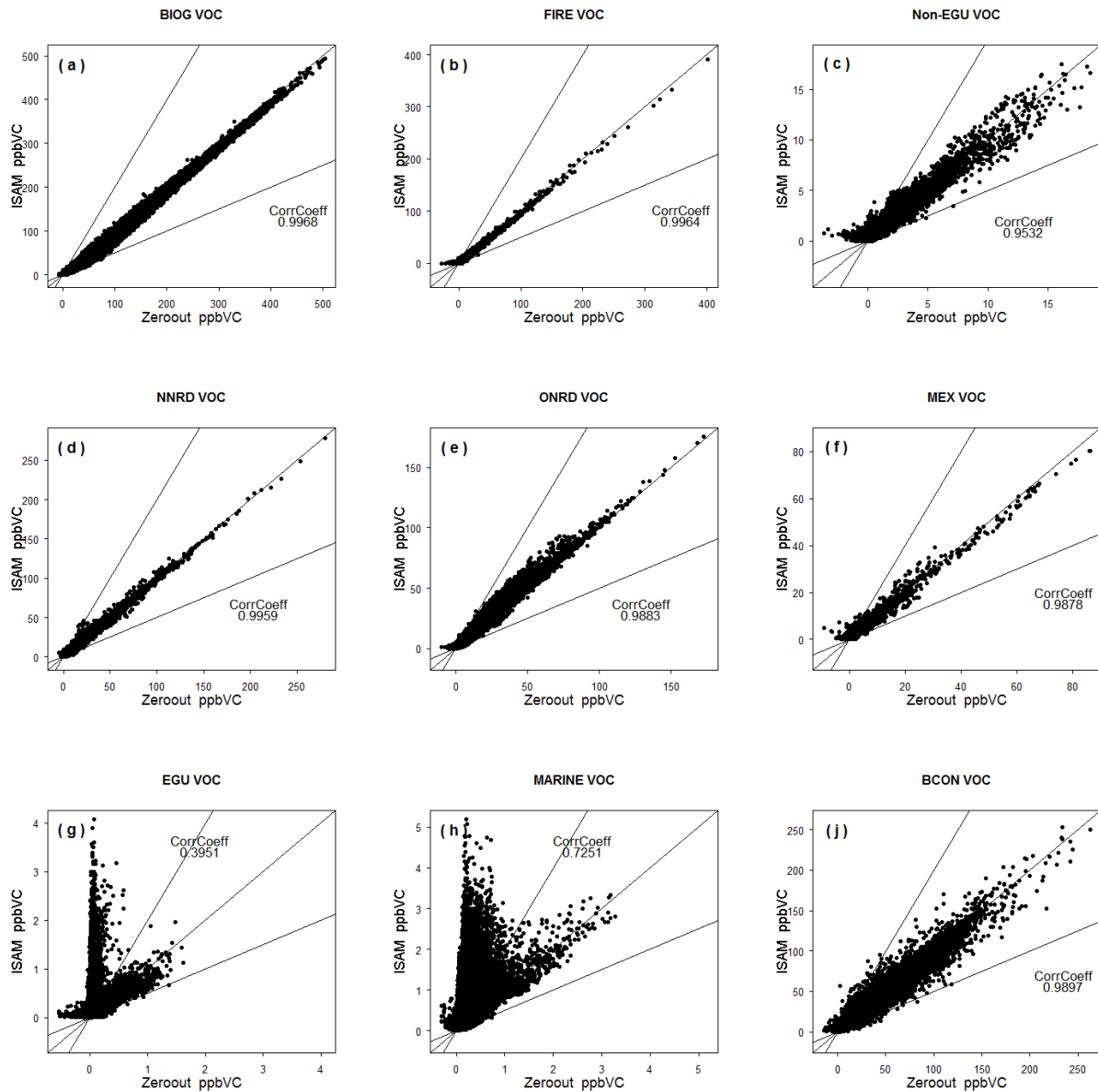


Figure 8. ISAM/V-out VOC comparison for each sector and all simulated hours. The sectors are: (a) biogenic BIOG, (b) wild fires FIRE, (c) non-electricity generation units Non-EGU, (d) non-road mobile NNRD, (e) on-road mobile ONRD, (f) other point sources MEX, (g) electricity generation units EGU, (h) marine MARINE, and (j) boundary conditions BCON. Note different scales across the panels.

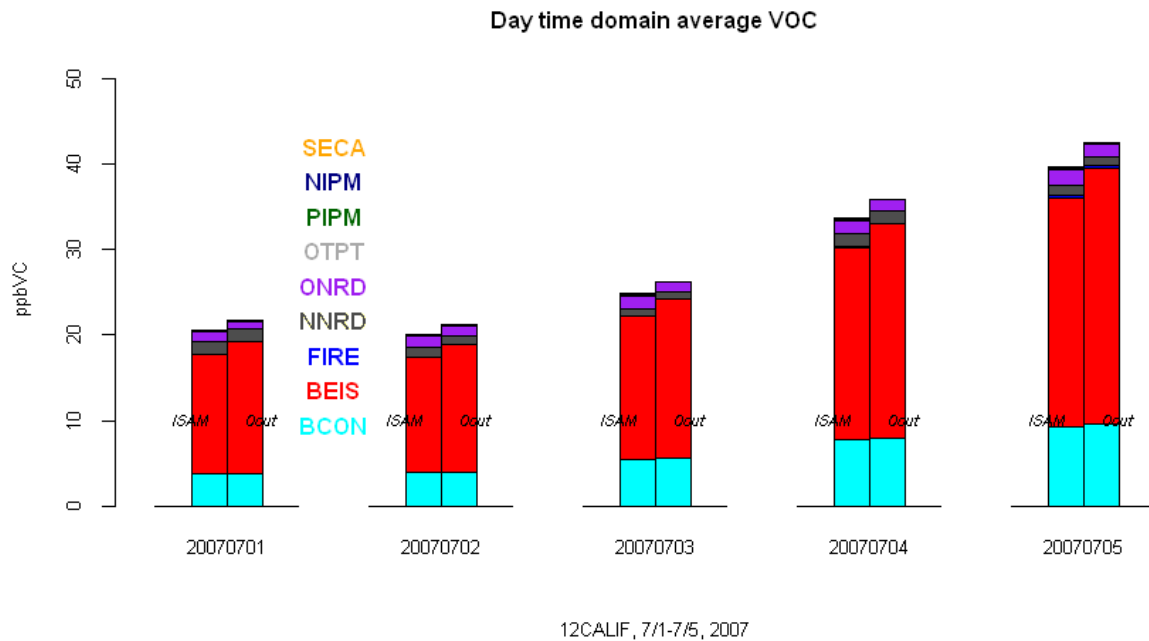


Figure 9. Daytime domain-averaged ambient VOC, July 1-5, 2007 (June 28-30 excluded due to large initial conditions influence). As in Fig. 4, for each day left column designates ISAM total, and right one the zero-out. The colors represent sector sources: marine (MARINE orange), non-electricity generation units (Non-EGU deep blue), electricity generation units (EGU green), other point sources (MEX light grey), on-road mobile (ONRD purple), non-road mobile (NNRD yellow), wild fires (FIRE blue), biogenic (BIOG red), and boundary conditions (BCON cyan).